Received: 23 September 2023 | Revised: 20 October 2023 | Accepted: 13 November 2023 | Published online: 23 November 2023

RESEARCH ARTICLE

Archives of Advanced Engineering Science
2024, Vol. 2(3) 142–149
DOI: 10.47852/bonviewAAES32021775

Fast Optimization Method of Flexible Support Structure Based on Mathematical Model

Qianzheng Du[1], Guiqiong Luo[1], Xi Wang[1,*], Tao Wang[1], Guoqiang Fu[1] and Caijiang Lu[1]

[1]*School of Mechanical Engineering, Southwest Jiaotong University, China*

Abstract: In order to realize the rapid analysis and optimization of the flexible support structure, the parametric design method is used to establish the three-dimensional model. Basic dimension parameters of the flexible support structure are linked with external data sources, and the functional relationship between dimensions is established to ensure the rationality of the model. It only needs to change the data in the data source to realize the automatic update of the 3D model when the model needs to be reconstructed. Compared with the finite element method, the optimization model improves the efficiency of simulation analysis and optimization design. The model proposed in this paper can obtain the optimal solution by weighing the mass and deformation displacement of the structure.

Keywords: complaint joints, optimization, mathematical model, simulation

1. Introduction

Because flexible structures [1] have many advantages, in addition to vibration reduction, noise reduction, friction-free, and so on, flexible support structures are commonly used to replace traditional rigid structures [2, 3], and flexible structures are widely used [4, 5]. Therefore, it is necessary to study the optimal design of flexible mechanism. There are three common modeling and analysis methods for flexible mechanism: pseudo-rigid body method, finite element method (FEM), and structure matrix method.

The pseudo-rigid body model (PRBM) is usually the first choice for the research and analysis of flexure hinge mechanism [6]. Wang et al. [7] develop two simple and accurate PRBMs for generalized cross-spring pivots. Verotti [8] investigated the role played by the initial curvature in case of uniform primitive flexures. Venkiteswaran and Su [9] proposed a revolute–prismatic revolute PRBM, which is more complete than the traditional PRBM. Kong et al. [10] expanded and abstracted the single-axis notch flexure hinge into a multi-structure system composed of a 3-degrees of freedom (DOF) hinge and two rigid bodies. Vedant and Allison [11] presented a more general model. These models can be used for co-design studies of flexible structural members and are capable of modeling higher deflection of compliant elements. Lodagala et al. [12] analyzed the error of the flexible ammonium chain pseudo-rigid model in the range of length ratio $d/L < 10$.

The FEM is also a common method for analyzing flexure hinge mechanisms. Li et al. [13] reconstructed compliant revolute joints after topology optimization, and the finite element modeling of the reconstructed geometric models is carried out by ANSYS. Gräser et al. [14] present a high-precision compliant XY micro-positioning stage with flexure hinges capable of realizing a motion range of ±10 mm along both axes. Eastwood et al. [15] used FEM techniques; they presented a sensitivity analysis investigating how the performance of this contact-aided compliant mechanism is affected by its geometry and derived a kinematics and statics model for the joint. Ruiz et al. [16] proposed a procedure for the kinematic design of a 3-PRS compliant parallel manipulator of 3-DOF. Choi et al. [17] propose a piezo-driven XY stage with a monolithic compliant parallel mechanism for fully bidirectional operation. Tartaglia et al. [18] presented design rules for partially restrained connections. A comprehensive parametric study based on finite element analysis was carried out in this paper. Sarkar and Dutta [19] also used FEM to analyze the deflection of the compliant links during walk. Linß et al. [20] investigated geometric scaling with a parametric nonlinear FEM model for factors from 0.1 to 2. There are lots of researchers who use FEM to verify the complaint joints [21, 22]. However, the FEM cannot establish a specific analytical expression, so it cannot establish the relationship between the stiffness of the flexible mechanism and its basic dimension parameters, so that the physical meaning of the design variable cannot be explained reasonably.

The structural matrix method is inspired by the FEM, ultimately to obtain a flexibility or stiffness matrix model that can reflect the entire mechanism. Li et al. [23] present a new compliant universal joint using four identical generic sheet flexures and a long wire beam. The linear finite element analysis is further applied to verify the analytical model for different joints. Chi et al. [24] present kinetostatic models of planar compliant mechanisms with multinary rigid links, multinary joints, sliders, and multiple loops based on the chained beam constraint model. Guo et al. [25] present the design concept of a novel magnetic flexonic mobile node incorporating a compliant beam and permanent magnets, and a 2-D model for simulating the deformed shape of the compliant beam. Compliance-based matrix method [26] can be effectively applied to serial compliant mechanism, while its adoption in modeling parallel compliant mechanism needs to be carefully examined due to the

*Corresponding author: Xi Wang, School of Mechanical Engineering, Southwest Jiaotong University, China. Email: wangxi028@swjtu.edu.cn

Figure 1
Flexible support model

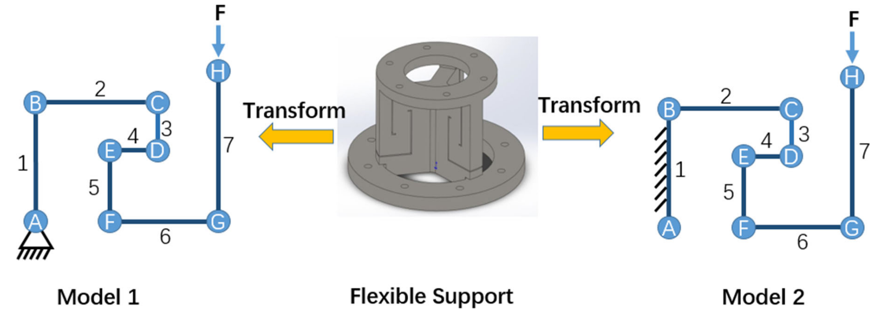

matrix inversion involved. Li and Zhu [27] presented an approach for designing compliant revolute joints based on a mechanism stiffness matrix using structural topology optimization. The structure matrix method has the advantage of speed in solving and is convenient for optimization design. Therefore, this paper chooses this method to construct and optimize the model.

In this paper, a mathematical model and a fast optimization method are established for the modeling and optimal design of flexible support structures. Compared with the traditional method and the FEM, the optimization design can be carried out more quickly. At the same time, the simulation accuracy can be ensured, and the optimal solution can be obtained by weighing the mass and deformation of the structure.

2. Mathematical Model of Flexible Support Structure

Most flexible mechanisms can be regarded as a structure composed of a series of plane flexible beams connected to each other [28]. The flexible support delineated in this paper can be conceptually represented by the mathematical formulation depicted in Figure 1. The flexible support structure is subject to a pair of constraints. One is that the structure corresponding to feature point A is connected to the bottom flange, so this position is a fixed constraint, forming the Model 1 as shown in Figure 1. Nevertheless, since the support plate in the middle of each support member is symmetrically distributed at 120°, the thickness of the central part of the whole structure is relatively large. Thus, a second constraint method is proposed, in which the beam 1 in the center of the overall structure is regarded as a fixed constraint, as shown in the Model 2 in Figure 1.

The subject of investigation pertains to a planar flexible beam exhibiting 3-DOF, comprising two translational motions and one rotational motion. As a consequence, its flexibility matrix assumes the form of a 3×3 matrix:

$$C = \begin{bmatrix} c_x & & \\ & c_y & c_{yz} \\ & c_{yz} & c_z \end{bmatrix} \tag{1}$$

where c_x is the axial deformation of the flexible beam in the direction of the unit axial (X direction) force, c_y is the tangential deformation in the direction of unit tangential (Y direction) force, and c_z represents the angle generated by the unit bending moment (γ direction). Due to the influence of tangential force, the beam undergoes bending, resulting in a bending angle. Similarly, the bending moment induces tangential deformation. As a result, there exist two additional coupled terms within the matrix. It is necessary to use the displacement reciprocity principle (also known as Maxwell's reciprocity principle) [29]; the value of two coupling terms is equal, expressed as c_{yz}.

In order to obtain the specific expression of each flexibility coefficient in formula (1), it is also necessary to combine Euler–Bernoulli beam theory, and then the expression of each element in the matrix is [30]:

$$\begin{cases} c_x = \frac{1}{EW}\int_0^L \frac{dx}{T(x)} \\ c_y = \frac{12}{EW}\int_0^L \frac{x^2dx}{T(x)^3} \\ c_z = \frac{12}{EW}\int_0^L \frac{dx}{T(x)^3} \\ c_{yz} = \frac{12}{EW}\int_0^L \frac{xdx}{T(x)^3} \end{cases} \tag{2}$$

where E is the Young's modulus of the material. W is the beam width, its direction is perpendicular to the surface of the paper. L is the axial length of the flexible beam. $T(x)$ indicates the tangential thickness of the beam at x length.

As shown in Figure 2, in a planar flexible mechanism containing n flexible beams, the mechanism is secured in the global coordinate system xy. The coordinate system x_iy_i pertains to a local coordinate system associated with beam i, while α_i denotes the angle between the two coordinate systems. All the external forces are acting on the characteristic points. The external forces at the feature point i include F_{ix},F_{iy}, and M_i. The displacement of the feature point i in the global coordinate system and the local coordinate system is (x_i, y_i, θ_i) and $(x_{li}, y_{li}, \theta_{li})$. The length and thickness of beam i are represented as L_i and T_i

Figure 2
Typical flexible structure

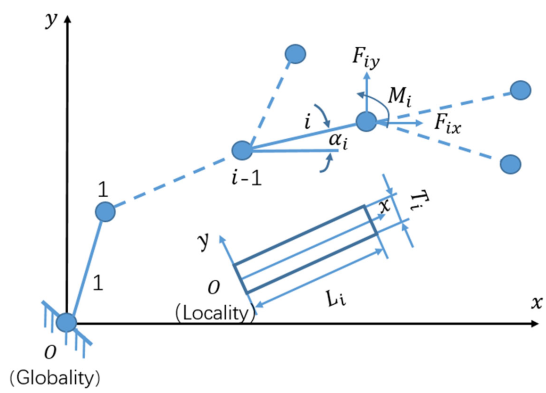

In accordance with the above description and the flexibility matrix, the deformation equation of beam i in local coordinate system can be obtained [28]:

$$c_{ix}\sum_{j\in\{i,CN_i\}}(F_{jx}\cos\alpha_i+F_{jy}\sin\alpha_i)=x_{li}-(x_{i-1}\cos\alpha_i+y_{i-1}\sin\alpha_i) \tag{3}$$

$$\begin{aligned}&c_{iy}\sum_{j\in\{i,CN_i\}}(F_{jy}\cos\alpha_i-F_{jx}\sin\alpha_i)\\&+c_{iyz}\{\sum_{j\in CN_i}[-F_{jx}\sum_{k\in BN_{i-j}}(L_k\sin\alpha_k)+F_{jy}\sum_{k\in BN_{i-j}}(L_k\cos\alpha_k)]+\sum_{j\in\{i,CN_i\}}M_j\}\\&=y_{li}-(-x_{i-1}\sin\alpha_i+y_{i-1}\cos\alpha_i)-L_i\theta_{i-1}\end{aligned} \tag{4}$$

$$\begin{aligned}&c_{iyz}\sum_{j\in\{i,CN_i\}}^{n}(F_{jy}\cos\alpha_i-F_{jx}\sin\alpha_i)\\&+c_{iz}\{\sum_{j\in CN_i}^{n}[-F_{jx}\sum_{k\in BN_{i-j}}^{j}(L_k\sin\alpha_k)+F_{jy}\sum_{k\in BN_{i-j}}^{j}(L_k\cos\alpha_k)]+\sum_{j\in\{i,CN_i\}}^{n}M_j\}\\&=\theta_{li}-\theta_{i-1}\end{aligned} \tag{5}$$

The above three equations are established for all n compliant beams and converted to matrix form [28]:

$$C_{1,3n\times 3n}F_{3n\times 1}=\begin{bmatrix}\cdots\\x_{li}-(x_{i-1}\cos\alpha_i+y_{i-1}\sin\alpha_i)\\y_{li}-(-x_{i-1}\sin\alpha_i+y_{i-1}\cos\alpha_i)-L_i\theta_{i-1}\\\theta_{li}-\theta_{i-1}\\\cdots\end{bmatrix} \tag{6}$$

where C_1 is the flexibility matrix of the entire structure in the local coordinate system, F is the external load matrix, and the dimensions of each matrix are represented by subscripts.

Subsequently, the equation is converted into global coordinates to ensure compliance with the rotational correlation between the global coordinate flexibility matrix and the local coordinate flexibility matrix:

$$C_{g,3n\times 3n}=\begin{bmatrix}\cdots&&&&\\&\cos\alpha_i&-\sin\alpha_i&0&\\&\sin\alpha_i&\cos\alpha_i&0&\\&0&0&1&\\&&&&\cdots\end{bmatrix} \tag{7}$$

Ultimately, by multiplying both sides of Equation (6) with the rotation matrix and conducting matrix transformations, the absolute displacement model can be derived:

$$C_{3n\times 3n}F_{3n\times l}=\begin{bmatrix}\cdots\\x_i\\y_i\\\theta_i\\\cdots\end{bmatrix}=U_{3n\times l} \tag{8}$$

where C is a flexibility matrix for the whole institution, F is the external load matrix, and U represents the displacement of all feature points in three directions.

3. Static Optimization Design

3.1. Mathematical model verification

In order to carry out statics optimization design, it is necessary to validate the correctness of the mathematical model constructed. The theoretical calculation outcomes of the Matlab-based mathematical model are juxtaposed with the results obtained from ANSYS simulation.

The width of the support part of the flexible support structure is 14.5 mm, and the Young's modulus is $E = 200$ Gpa. Other relevant values are shown in Table 1.

Take beam 4 as an example, the interval of variable setting is respectively: $0.1L_0 \le L \le L_0$, $0.1t_0 \le t \le t_0$, $0.5w_0 \le w \le 2w_0$, where L_0, t_0, w_0 represent the length, thickness, and width of beam 4 in the initial model.

As depicted in Figure 3, the mathematical model constructed is basically consistent with the analysis results of the ANSYS simulation model under the influence of different length, thickness, and width parameters. The relative error of the results falls within the range of 25%–30%, indicating the viability of the mathematical model.

To further corroborate the dependability of the mathematical model, the relationship between force and displacement of the flexible structure is simulated under a variety of pose conditions. Figure 4 shows the relationship between force and displacement of the flexible support structure when the tilt angle is 30°, 45°, 60°, and 90°. The displacement of the end of the flexible support increases with the rise of the tilt angle. Likewise, the results of the mathematical model are almost consistent with those of the ANSYS simulation model, and the error is not large. It is sufficient to demonstrate the reliability of the mathematical model. It is evident from the figure that the mathematical analysis outcomes of Model 2 exhibit closer agreement with the ANSYS finite element analysis. Consequently, the subsequent optimization design will be primarily based on Model 2.

3.2. Mathematical model optimization design

Optimal design can be expressed as formulating the objective function under given constraints to calculate the optimal solution. Based on the actual conditions of the flexible support structure, the optimal mathematical model is formulated. By converting its

Table 1
Some basic parameters of flexible support structure

	Beam 1	Beam 2	Beam 3	Beam 4	Beam 5	Beam 6	Beam 7
Length	52 mm	18 mm	17 mm	2.7 mm	18 mm	15.5 mm	46.5 mm
Thickness	48 mm	16 mm	13 mm	17.5 mm	13 mm	16.5 mm	11 mm
Angle	90°	0°	-90°	90°	-90°	0°	90°

Figure 3
Relation between force and displacement of beam 4 under different parameters

(a) Relation between length and displacement

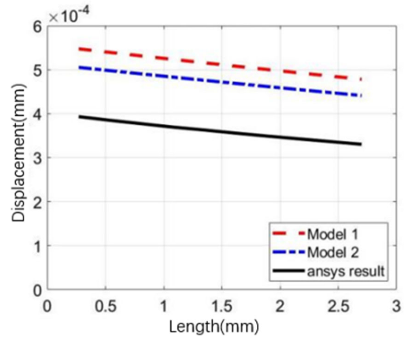

(b) Relation between thickness and displacement

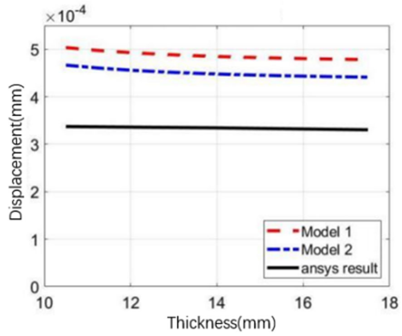

(c) Relation between width and displacement

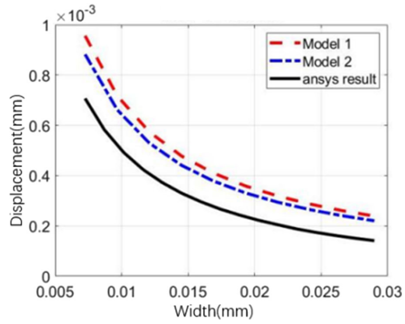

Figure 4
Relation between force and displacement under different tilt angles

(a) 30° tilt condition

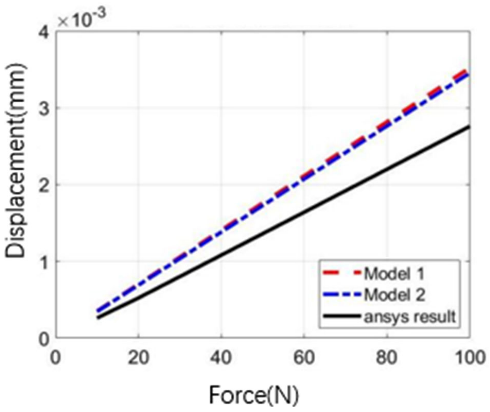

(b) 45° tilt condition

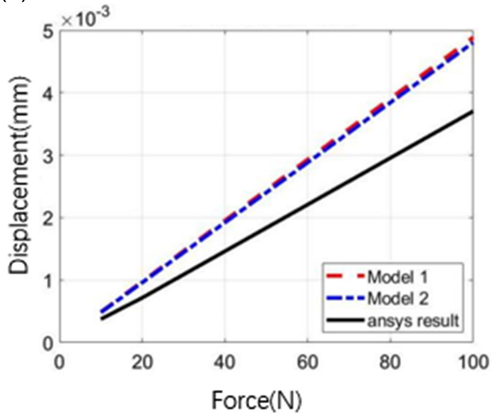

(c) 60° tilt condition

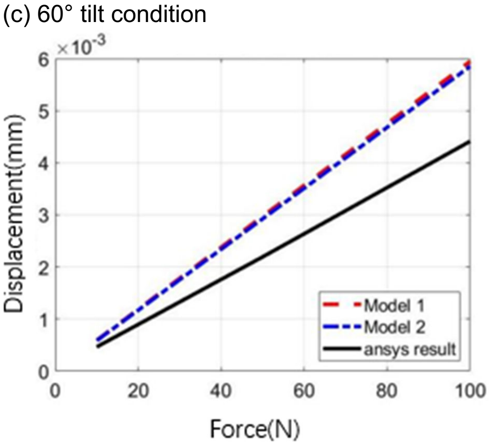

(d) 90° tilt condition

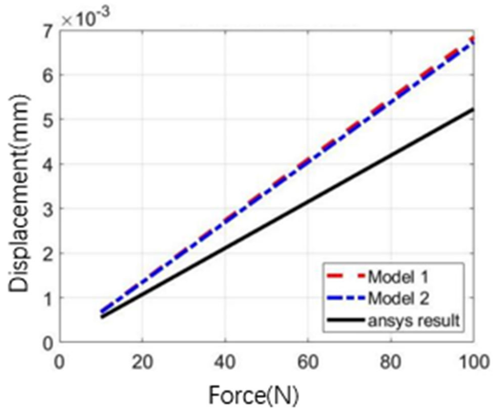

end displacement into an objective function with constraints, the structural optimization problem can be expressed as [28]:

$$\begin{cases} \min f(X) \\ X = \{X_1, X_2, ..., X_n\} \\ s.t. \quad g_v(X) \le 0, (v = 1, 2, ..., m) \\ \qquad h_u(X) = 0, (u = 1, 2, ..., p) \end{cases} \tag{9}$$

where $X = \{X_1, X_2, ..., X_n\}$ is a design variable, $f(X)$ is the objective function, $g_v(X)$ represents inequality constraints, and $h_u(X)$ represents equality constraints.

Thirteen fundamental dimension parameters are chosen as design variables based on Model 2. The range of these 13 variables defines the constraints in terms of upper and lower bounds, which can be expressed as follows:

$$\begin{cases} ub = [27, 25.5, 4.05, 27, 23.25, 69.75, 24, 19.5, 26.25, 19.5, 24.75, 16.5, 29] \\ lb = [14.4, 13.6, 2.16, 14.4, 12.4, 37.2, 12.8, 10.4, 14, \ 10.4, \ 13.2, \ 8.8, \ 7.25] \end{cases} \tag{10}$$

where *ub* is the upper bound of variable values, and *lb* is the lower bound of the variable value. The final optimization result range is between the upper bound and the lower bound, which can be denoted as:

$$g_v(X) \le 0 \qquad (v = 1, 2, ..., 26) \tag{11}$$

The flexible support structure is distinguished by the presence of gaps between each support beam. The imposed constraints will guarantee that the width of these gaps remains greater than or equal to 0.5 mm. The constraints are as follows:

$$\begin{cases} L_3 + L_5 - L_7 + 0.5t_2 \le -2.7 \\ L_4 - L_6 + 0.5t_3 + 0.5t_7 \le -0.5 \\ -L_2 + L_4 + 0.5t_5 \le -8.5 \\ -L_5 + 0.5t_2 + 0.5t_4 \le -0.5 \\ -L_5 + 0.5t_4 + t_6 \le -0.5 \\ -L_6 + 0.5t_5 + 0.5t_7 \le -1 \end{cases} \tag{12}$$

The parameters within the equation form a subset of the design variable parameters, and their functional relationship is derived based on the dimensional interdependencies within the three-dimensional model, and it is denoted by the mathematical model representation method:

$$g_v(X) \le 0 \qquad (v = 27, 28, \ldots, 32) \tag{13}$$

After meeting the reasonable parameters of the flexible support structure, it is also essential to constrain its overall mass. When defining the constraints related to the quality, a specific flexible support component is chosen as the focus of the research. The volume expression of the support part is as follows:

$$\begin{cases} S_1 = (52 - 0.5t_2) \times 16 \\ S_2 = (8 + L_2 + 0.5t_3) \times t_2 \\ S_3 = (0.5t_5 + L_6 + 0.5t_7) \times t_6 \\ S_4 = (L_7 - 0.5t_6) \times t_7 \\ S_5 = (L_3 - 0.5t_2 - 0.5t_4) \times t_3 \\ S_6 = (L_5 - 0.5t_6 - 0.5t_4) \times t_5 \\ S_7 = (0.5t_5 + L_4 + 0.5t_3) \times t_4 \\ V = (S_1 + S_2 + S_3 + S_4 + S_5 + S_6 + S_7) \times w \end{cases} \tag{14}$$

After obtaining the volume of the support part, the constraints sets are as follows:

$$\begin{cases} c = V - V_0 \\ c_{eq} = [] \end{cases} \tag{15}$$

The constraint condition is expressed as:

$$g_v(X) \le 0 \quad (v = 33) \tag{16}$$

According to the above derivation, the final optimization model can be obtained as follows:

$$\begin{cases} \min D(X) \\ X = \{X_i\} \quad (i = 1, 2, ..., 13) \\ s.t. \quad g_v(X) \le 0 \quad (v = 1, 2, ..., 33) \end{cases} \tag{17}$$

The fundamental dimensional parameters of the flexible support structure were optimized using a rapid optimization approach based on the mathematical model. The solution results are stored in the data source file of the parametric 3D model to facilitate the inverse solution of the 3D model. The structure comparison of 3D models before and after optimization is shown in Figure 5.

As is shown in Figure 6, when the nonlinear constraint targets were 80%, 100%, and 120% of the total mass before optimization, the structure of the support part changed. Referring to Table 2, the length parameter L and thickness parameter t of each beam of the

Figure 5
The comparison of front and rear flexible support structures was optimized

(a) Flexible support structure model before optimization

(b) The optimized flexible support structure model

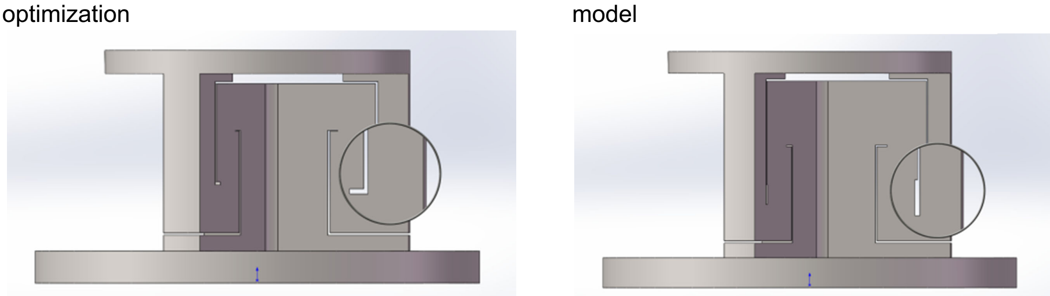

Figure 6
Optimization results of support structures under different mass constraints

(a) The mass is 80% of that before optimization
(b) The mass is the same as that before optimization
(c) The mass is 120% of that before optimization

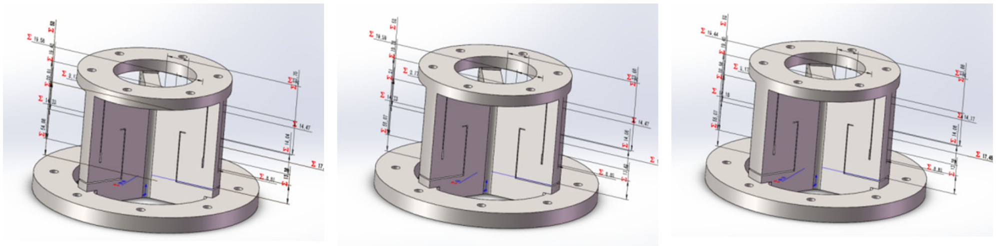

Figure 7
The relationship between force and displacement after mass change

(a) The mass is 80% before optimization
(b) The mass is the same as before optimization
(c) The mass is 120% of that before optimization

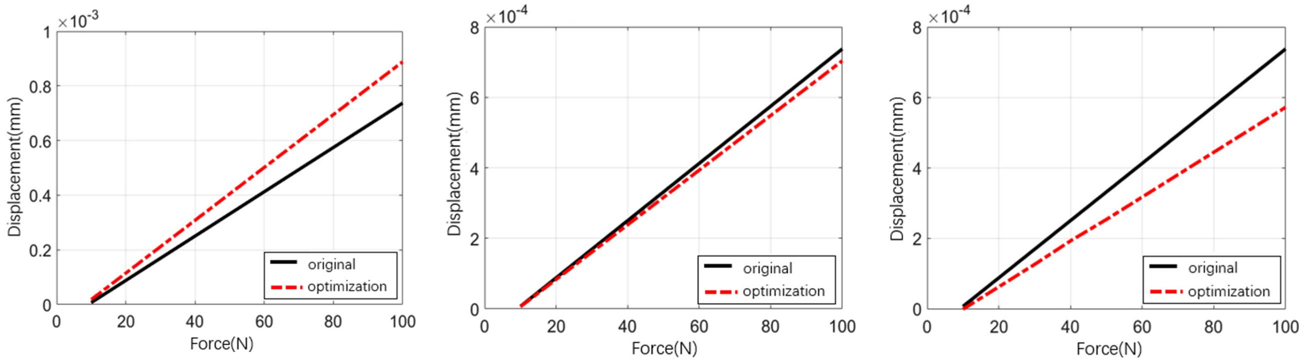

Table 2
Optimization results of design variables under different quality constraints

	Quality is 80% before optimization/mm	The quality is the same as before optimization/mm	The quality is 120% of that before optimization/mm
L_2	19.5773	19.5886	19.4357
L_3	19.3961	19.3752	19.4017
L_4	2.1685	2.1732	2.1724
L_5	20.9109	21.0022	20.9592
L_6	14.3169	14.3283	14.1760
L_7	54.9773	55.0681	55.0687
t_2	23.6968	23.6021	23.6555
t_3	14.4708	14.4697	14.1690
t_4	14.0402	14.0624	14.0608
t_5	17.7687	17.7550	17.4527
t_6	13.3606	13.4239	13.3834
t_7	8.8109	8.8170	8.8161
w	10.4	13	15.7

flexible support structure have certain changes under different mass conditions. But the change amplitude is small. The width parameter w of the support part has the largest variation. Under parametric design and nonlinear constraint conditions, the width parameter w plays a crucial role in determining the quality outcome. Its variations have a significant impact on the overall quality of the structure.

Upon obtaining the optimal solution, the three-dimensional model is generated, and the model optimized by the flexible support structure is simulated and analyzed using ANSYS software. The feasibility of the optimization method is verified by comparing with the simulation results before optimization. As shown in Figure 7(b), when the constrained mass is the same as the model mass prior to optimization, it is observed that the end displacement of the optimized model exhibits a marginal reduction compared to the pre-optimized state under identical loading conditions. This indicates that the rapid optimization design approach based on mathematical models has succeeded in optimizing the objective function while also meeting the desired design specifications. The relationship between force and displacement under different mass constraints is analyzed in Figure 7(a) and (c). Within the size constraint, the larger the mass is, the smaller the end displacement of the support structure and the more obvious the optimization effect are.

4. Conclusion

In this paper, the modeling and optimal design of flexible support structures are studied. It involves the parametric design of 3D model, the research of tree structure model based on linear beam theory, and the establishment of mathematical optimization design model. It provides a thought for the study of flexible support structure optimization. With accuracy being the primary consideration, three optimization outcomes are achieved based on different quality constraints. The results show that the end displacement of the optimized model is smaller than that before optimization when the mass is the same before and after optimization. It shows that the optimization mathematical model proposed in this paper has the ability of fast optimization. Combined with the other two cases, it can be concluded that the larger the mass of the flexible support structure in this paper, the smaller the end displacement. In practical engineering, the model is capable of achieving an optimal solution by striking a balance between displacement and mass.

Funding Support

The authors gratefully acknowledge the support from National Natural Science Foundation of China (52005417) and Sichuan Science and Technology Program (2023NSFSC0858).

Ethical Statement

This study does not contain any studies with human or animal subjects performed by any of the authors.

Conflicts of Interest

The authors declare that they have no conflicts of interest to this work.

Data Availability Statement

Data sharing is not applicable to this article as no new data were created or analyzed in this study.

References

[1] Wu, X., Lu, Y., Duan, X., Zhang, D., & Deng, W. (2019). Design and DOF analysis of a novel compliant parallel mechanism for large load. *Sensors*, *19*(4), 828. https://doi.org/10.3390/s19040828

[2] Branz, F., & Francesconi, A. (2023). Compliant joint to reduce docking loads between CubeSats. *Acta Astronautica*, *205*, 153–162. https://doi.org/10.1016/j.actaastro.2023.01.035

[3] Zhang, J., Lu, K., Chen, W., Jiang, J., & Chen, W. (2015). Monolithically integrated two-axis microgripper for polarization maintaining in optical fiber assembly. *Review of Scientific Instruments*, *86*(2). https://doi.org/10.1063/1.4907551

[4] Venkiteswaran, V. K., & Su, H. J. (2018). A versatile 3R pseudo-rigid-body model for initially curved and straight compliant beams of uniform cross section. *Journal of Mechanical Design*, *140*(9). https://doi.org/10.1115/1.4040628

[5] Wang, F., Liang, C., Tian, Y., Zhao, X., & Zhang, D. (2015). Design of a piezoelectric-actuated microgripper with a three-stage flexure-based amplification. *IEEE/ASME Transactions on Mechatronics*, *20*(5), 2205–2213. https://doi.org/10.1109/TMECH.2014.2368789

[6] Šalinić, S., & Nikolić, A. (2018). A new pseudo-rigid-body model approach for modeling the quasi-static response of planar flexure-hinge mechanisms. *Mechanism and Machine Theory*, *124*, 150–161. https://doi.org/10.1016/j.mechmachtheory.2018.02.011

[7] Wang, Z., Sun, H., Wang, B., & Wang, P. (2014). Adaptive pseudo-rigid-body model for generalized cross-spring pivots under combined loads. *Advances in Mechanical Engineering*, *12*(12). https://doi.org/10.1177/1687814020966539

[8] Verotti, M. (2018). Effect of initial curvature in uniform flexures on position accuracy. *Mechanism and Machine Theory*, *119*, 106–118. https://doi.org/10.1016/j.mechmachtheory.2017.08.021

[9] Venkiteswaran, V. K., & Su, H. J. (2015). Development of a 3-spring pseudo rigid body model of compliant joints for robotic applications. In *ASME Design Engineering Technical Conferences and Computers and Information in Engineering Conference*.

[10] Kong, N., Sanders, A., & Wulfsberg, J. P. (2015). On the design methodology of flexure-based compliant mechanisms by utilizing pseudo-rigid-body models with 3-DOF joints. In *Proceedings of the 14th IFToMM World Congress*, 631–637.

[11] Vedant, & Allison, J. T. (2020). Pseudo-rigid-body dynamic models for design of compliant members. *Journal of Mechanical Design*, *142*(3).

[12] Lodagala, V., Karthik, K., & Midha, A. (2016). Limitations in the use of small-length flexural pivot in a pseudo-rigid-body model. In *International Design Engineering Technical Conferences and Computers and Information in Engineering Conference*.

[13] Li, L., Geng, Z., & Zhong, B. (2017). Design and optimization of compliant revolute joint based on finite element method, intelligent computing. In *Networked Control, and Their Engineering Applications*, 115–124.

[14] Gräser, P., Linß, S., Harfensteller, F., Torres, M., Zentner, L., & Theska, R. (2021). High-precision and large-stroke XY micropositioning stage based on serially arranged compliant mechanisms with flexure hinges. *Precision Engineering*, *72*, 469–479. https://doi.org/10.1016/j.precisioneng.2021.02.001

[15] Eastwood, K. W., Francis, P., Azimian, H., Swarup, A., Looi, T., Drake, J. M., & Naguib, H. E. (2018). Design of a contact-aided compliant notched-tube joint for surgical manipulation in confined workspaces. *Journal of Mechanisms and Robotics*, *10*(1). https://doi.org/10.1115/1.4038254

[16] Ruiz, A., Campa, F. J., Roldán-Paraponiaris, C., Altuzarra, O., & Pinto, C. (2016). Experimental validation of the kinematic design of 3-PRS compliant parallel mechanisms. *Mechatronics*, *39*, 77–88. https://doi.org/10.1016/j.mechatronics.2016.08.006

[17] Choi, K., Lee, J., Kim, G., Lim, H., Kwon, S., & Lee, S. C. (2020). Design and analysis of a flexure-based parallel XY stage driven by differential piezo forces. *International Journal of Precision Engineering and Manufacturing*, *21*, 1547–1561. https://doi.org/10.1007/s12541-020-00358-0

[18] Tartaglia, R., D'Aniello, M., & Rassati, G. A. (2019). Proposal of AISC-compliant seismic design criteria for ductile partially-restrained end-plate bolted joints. *Journal of Constructional Steel Research*, *159*, 364–383. https://doi.org/10.1016/j.jcsr.2019.05.006

[19] Sarkar, A., & Dutta, A. (2018). Optimal trajectory generation and design of an 8-DoF compliant biped robot for walk on inclined ground. *Journal of Intelligent & Robotic Systems*, *94*, 583–602.

[20] Linß, S., Gräser, P., Räder, T., Henning, S., Theska, R., & Zentner, L. (2018). Influence of geometric scaling on the elasto-kinematic properties of flexure hinges and compliant mechanisms. *Mechanism and Machine Theory*, *125*, 220–239. https://doi.org/10.1016/j.mechmachtheory.2018.03.008

[21] Eastwood, K. W., Swarup, A., Francis, P., Alvara, A. N., Chen, H., Looi, T., . . . , & Drake, J. M. (2020). A steerable neuroendoscopic instrument using compliant contact-aided joints and monolithic articulation. *Journal of Medical Devices*, *14*(2). https://doi.org/10.1115/1.4045934

[22] Sun, Y., & Lueth, T. C. (2021). Cruciate-ligament-inspired compliant joints: Application to 3D-printed continuum surgical robots. In *2021 43rd Annual International Conference of the IEEE Engineering in Medicine & Biology Society*, 4645–4648.

[23] Li, S., Hao, G., & Wright, W. M. D. (2021). Design and modelling of an anti-buckling compliant universal joint with a compact configuration. *Mechanism and Machine Theory*, *156*. https://doi.org/10.1016/j.mechmachtheory.2020.104162

[24] Chi, I. T., Chang, P. L., Tran, N. D. K., & Wang, D. A. (2021). Kinetostatic modeling of planar compliant mechanisms with flexible beams, linear sliders, multinary rigid links, and multiple loops. *Journal of Mechanisms and Robotics*, *13*(5). https://doi.org/10.1115/1.4050196

[25] Guo, J., Lee, K. M., Zhu, D., Yi, X., & Wang, Y. (2012). Large-deformation analysis and experimental validation of a flexure-based mobile sensor node. *IEEE/ASME Transactions on Mechatronics*, *17*(4), 606–616. https://doi.org/10.1109/TMECH.2011.2107579

[26] Wang, J., Yang, Y., Yang, R., Feng, P., & Guo, P. (2019). On the validity of compliance-based matrix method in output compliance modeling of flexure-hinge mechanism. *Precision Engineering*, *56*, 485–495. https://doi.org/10.1016/j.precisioneng.2019.02.006

[27] Li, L., & Zhu, X. (2019). Design of compliant revolute joints based on mechanism stiffness matrix through topology optimization using a parameterization level set method. *Structural and Multidisciplinary Optimization*, *60*, 1475–1489.

[28] Niu, M., Yang, B., Yang, Y., & Meng, G. (2018). Two generalized models for planar compliant mechanisms based on tree structure method. *Precision Engineering*, *51*, 137–144. https://doi.org/10.1016/j.precisioneng.2017.08.002

[29] Ugural, A. C., & Fenster, S. K. (2003). *Advanced strength and applied elasticity*. UK: Prentice Hall.

[30] Lobontiu, N. (2002). *Compliant mechanisms: Design of flexure hinges*. USA: CRC Press.

How to Cite: Du, Q., Luo, G., Wang, X., Wang, T., Fu, G., & Lu, C. (2024). Fast Optimization Method of Flexible Support Structure Based on Mathematical Model. *Archives of Advanced Engineering Science*, *2*(3), 142–149. https://doi.org/10.47852/bonviewAAES32021775